Supporting Information for

Enhancing the hydrophobicity of perovskite solar cells using C18 capped $CH_3NH_3PbI_3$ nanocrystals

Isabella Poli,[§] [‡] *Xinxing Liang,* [§] *Robert Baker,* [§] [‡] *Salvador Eslava,*[¶] [‡] *and Petra Cameron*[§] [‡]

[§]*Department of Chemistry, University of Bath, Bath BA2 7AY, United Kingdom*

[¶]*Department of Chemical Engineering, University of Bath, Bath BA2 7AY, United Kingdom*

[‡]*Centre for Sustainable Chemical Technologies, University of Bath, Bath BA2 7AY, United Kingdom*

Experimental

Characterisation

Cyclic Voltammetry Cyclic Volatmmetry (CV) scans were performed in a dichloromethane (DCM) solution of 0.1 M Bu_4NPF_6 at a scan rate of $20\,mV\,s^{-1}$. Ag/AgCl was used as reference electrode and Pt as counter electrode. The oxidative peak potential of Ag/AgCl *vs* the normal hydrogen electrode (NHE) is set to 0.197 V and the NHE *vs* the vacuum level to 4.5 V [1]. The VB level was calculated according to the formula VB=-(E^{ox}+4.697) eV. The oxidation potential E^{ox} was calculated from the onset potential of the redox wave.

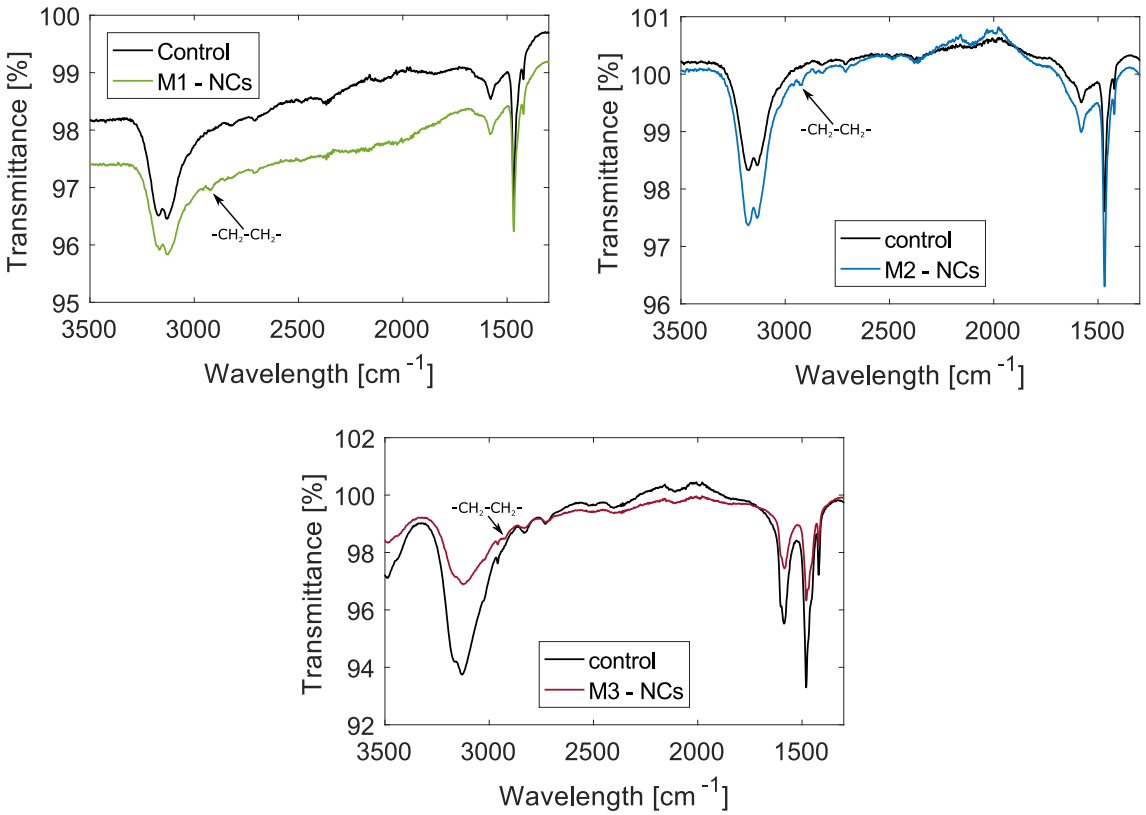

Fig. S1: FTIR spectra of perovskite films with and without MAPI NCs incorporated using methods M1, M2 and M3

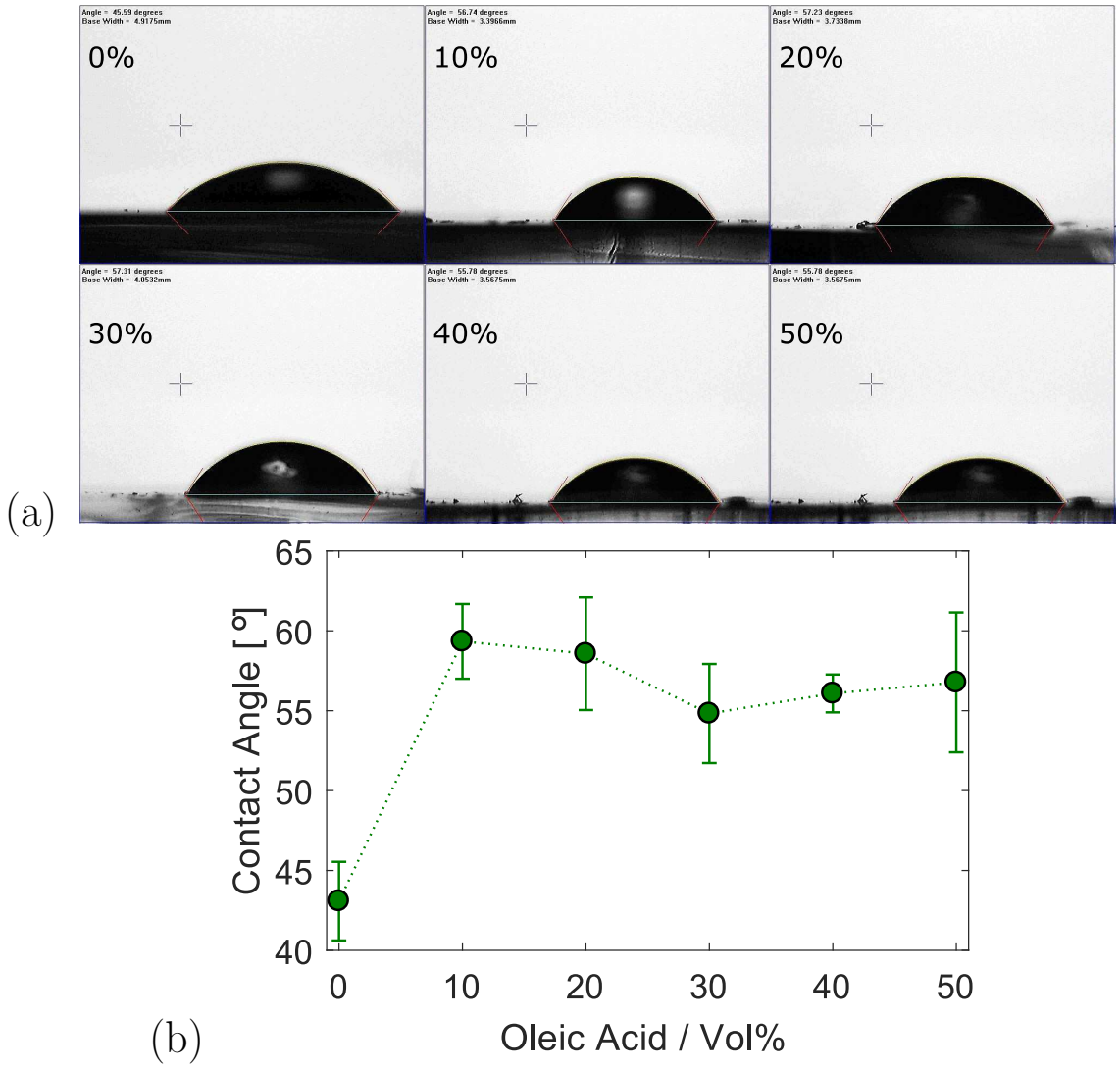

Fig. S2: (a) Surface water contact angles of perovskite films with different concentration of OA in toluene; (b) variation of the contact angle with the concentration of OA in toluene.

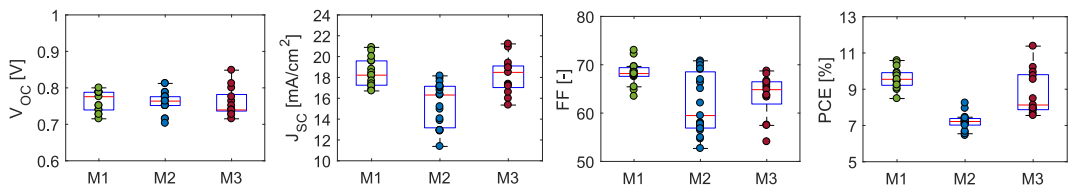

Fig. S3: Photovoltaic parameters shown as box plots for efficiency distributions of standard perovskite solar cells fabricated using three different deposition techniques. Cells have been tested under AM 1.5 and 1 sun illumination. The reproducibility is evaluated by characterising 15, 19 and 13 cells for M1, M2 and M3 respectively

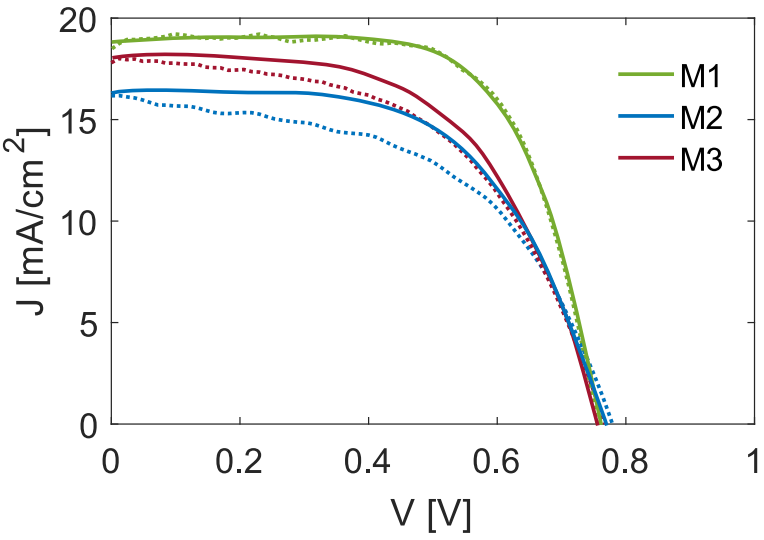

Fig. S4: JV curves of average performing solar cells deposited via the three different methods M1, M2 and M3. The solid line is the curve measured under reverse scan, while the dotted line is the one measured under forward scan.

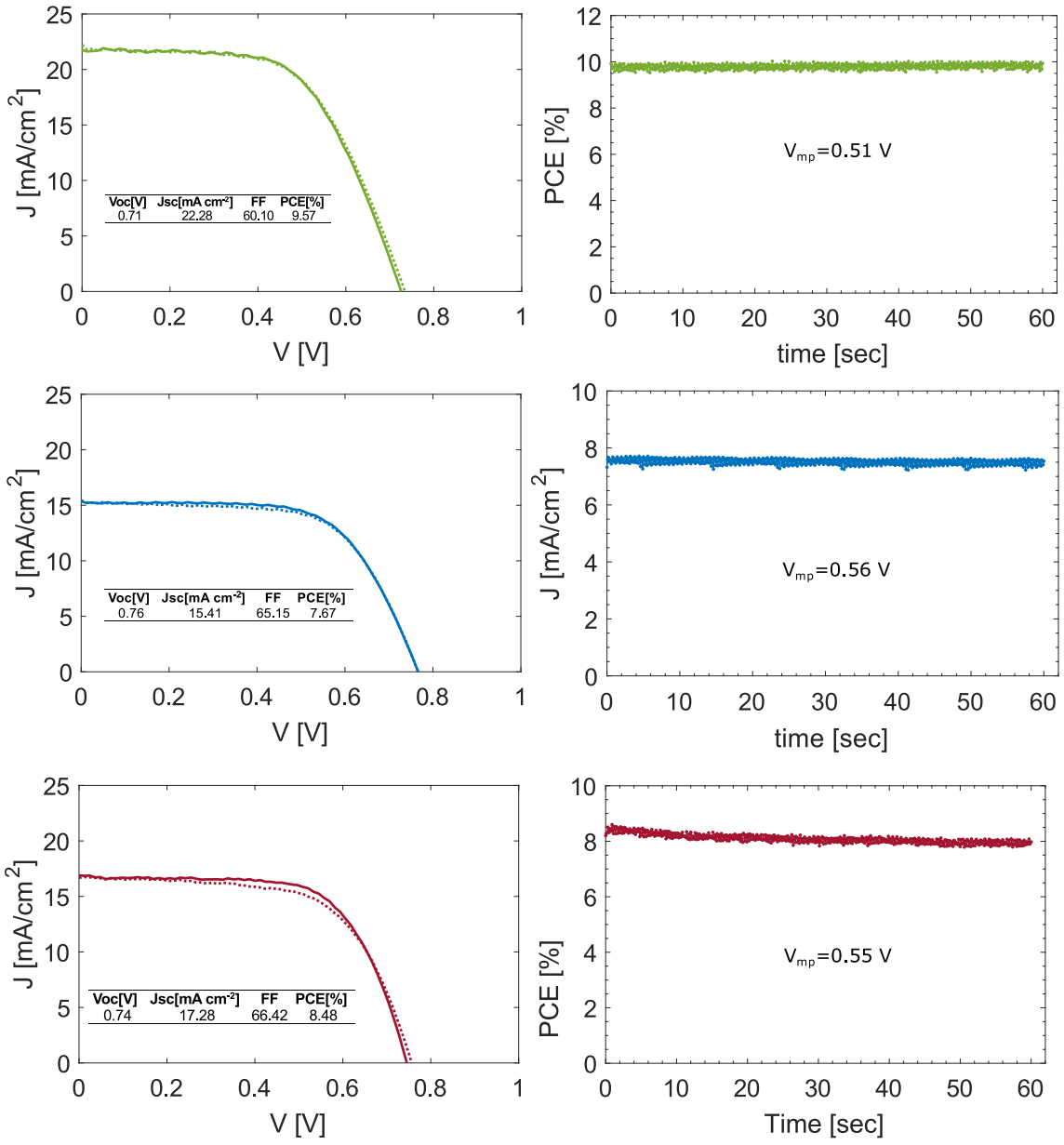

Fig. S5: JV curves of solar cells deposited via the three different methods M1, M2 and M3 (from top to bottom). Stabilised power conversion efficiency was measured by applying the maximum voltage point calculated during the JV scan for 60 seconds

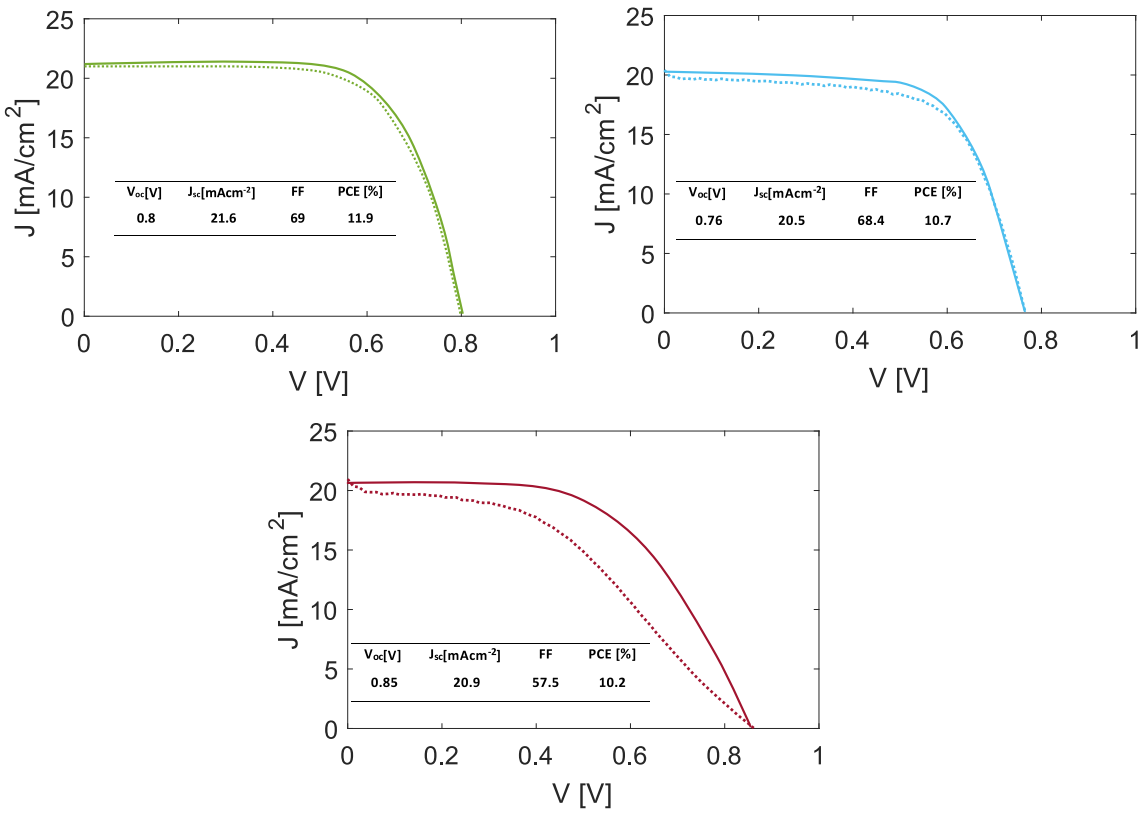

Fig. S6: JV curves of control mesoporous devices (without MAPI NCs) deposited via the three different methods M1, M2 and M3 (from top to bottom)

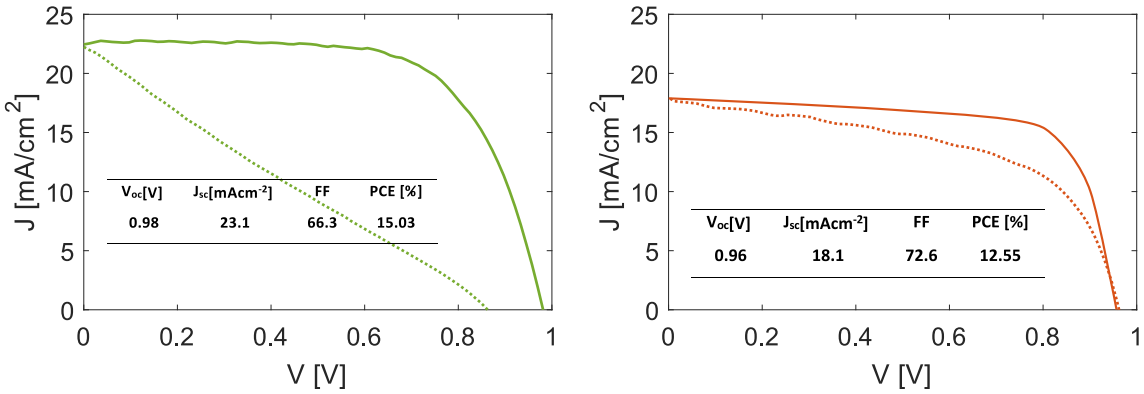

Fig. S7: JV curves of control standard planar device (left) and inverted cell (right)

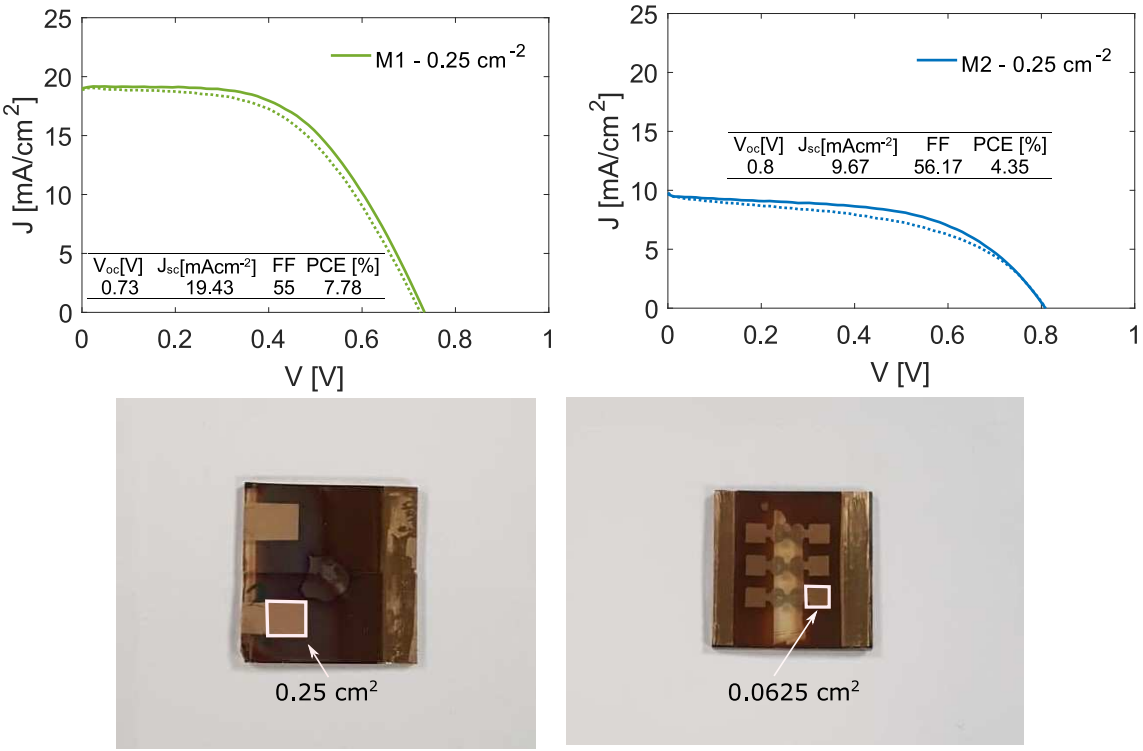

Fig. S8: JV curves and pictures of perovskite solar cells fabricated using method M1 and M2. The active area is 0.25 cm^2.

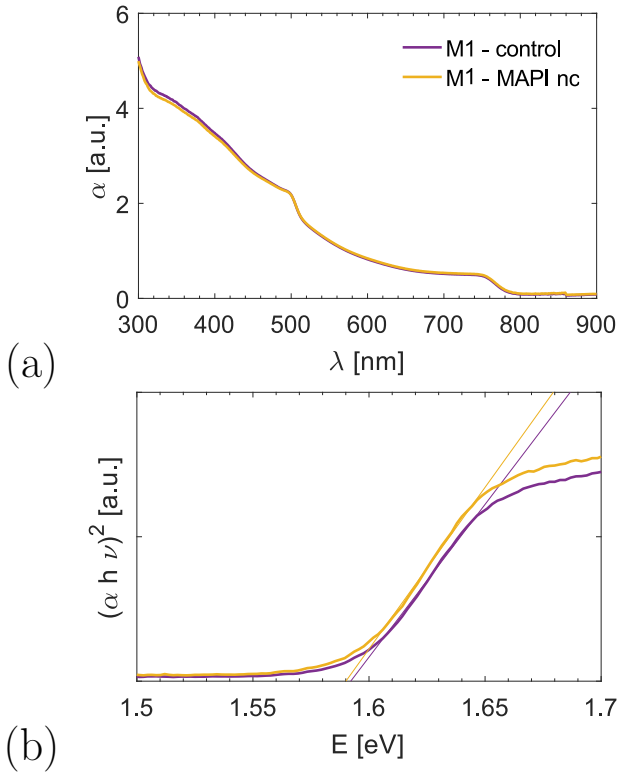

Fig. S9: (a) UV-vis absorption and (b) Tauc plot of perovskite films without and with the incorporated MAPI NCs

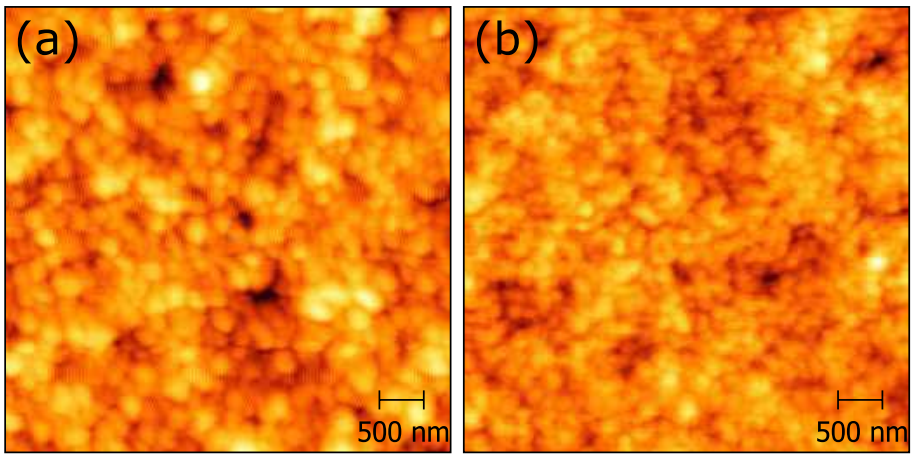

Fig. S10: AFM images of perovskite films (a) without and (b) with integrated MAPI NCs. Films deposited by using the second deposition method M2

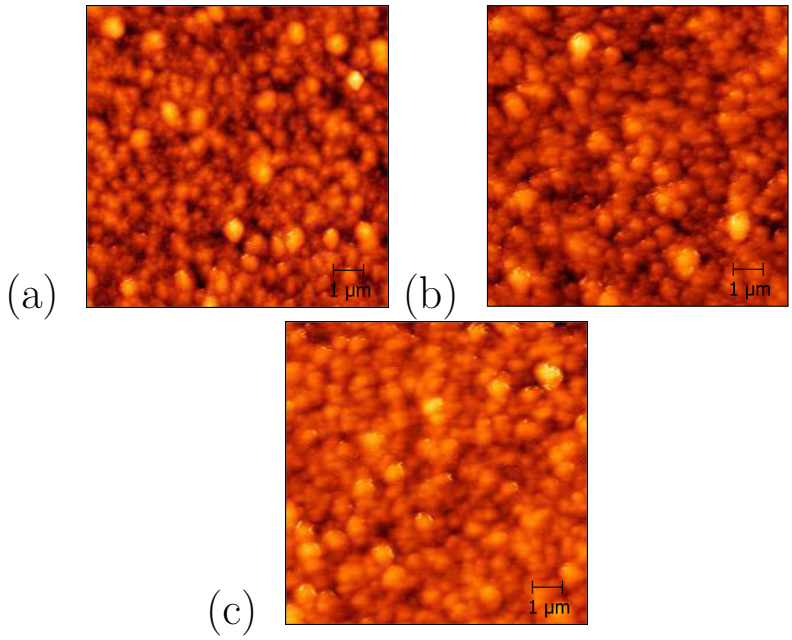

Fig. S11: AFM images of perovskite films with integrated MAPI NCs. The MAPI NCs dispersed in toluene solution was diluted in order to obtain less concentrated solutions (NCs+toluene:toluene-65:35 and NCs+toluene:toluene-30:70) (a) NCs+toluene:toluene - 30:70 (b) NCs+toluene:toluene - 65:35 (c) NCs+toluene:toluene - 100:0

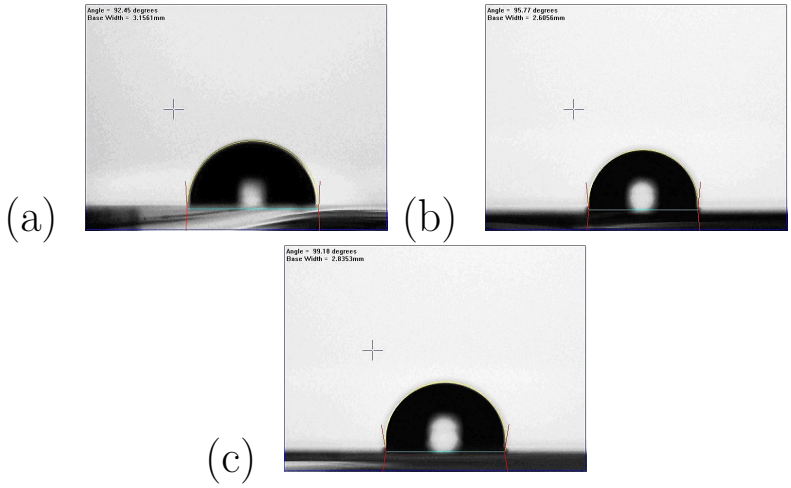

Fig. S12: Surface water contact angle of perovskite films with integrated MAPI NCs. Different concentration of the MAPI NCs solution is used: (a) NCs+toluene:toluene - 30:70 (92°) (b) NCs+toluene:toluene - 65:35 (96°) (c) NCs+toluene:toluene - 100:0 (99°)

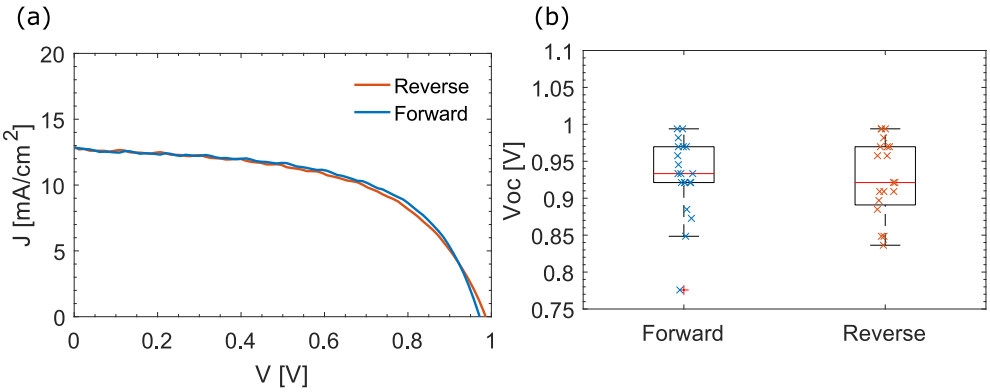

Fig. S13: (a) JV curves of an inverted structure perovskite solar cell without MAPI NCs incorporated at the $CH_3NH_3PbI_3$/PCBM interface; (b) Comparison of the open circuit voltages measured by the forward and reverse scan for control cells with inverted architecture

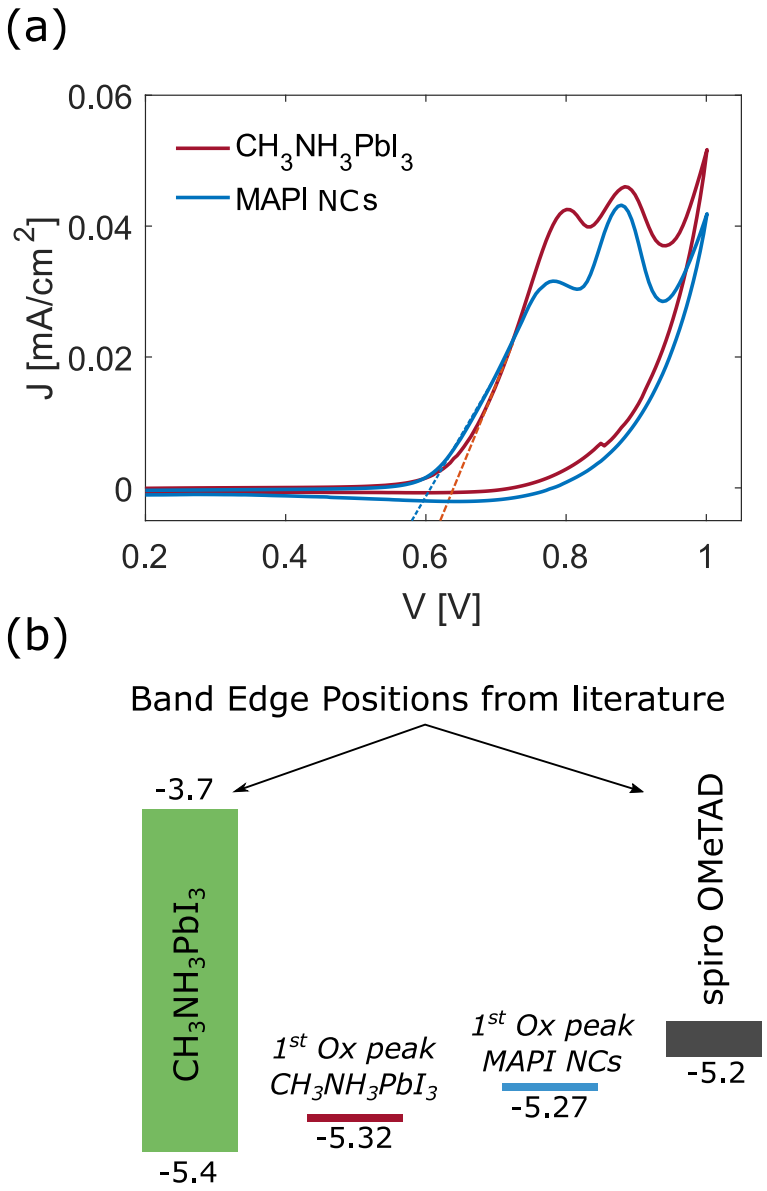

Fig. S14: (a) cyclic voltammetry data of perovskite and perovskite/MAPI NCs (fabricated by using M1) in a DCM solution of 0.1 M Bu_4NPF_6 at a scan rate of 20 mV/s; (b) Comparison of the band edge positions of $CH_3NH_3PbI_3$ and spiro-OMeTAD and the position of the first oxidation peaks detected for the studied materials

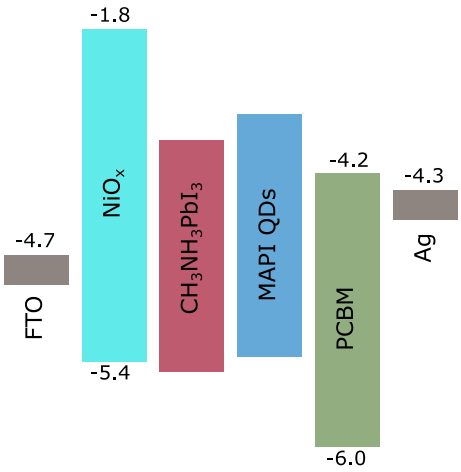

Fig. S15: sketch of the energy band diagram of an inverted architecture. Higher CB position of MAPI NCs might create an extraction barrier at the interface that could cause the inverted hysteresis phenomenon

(a) 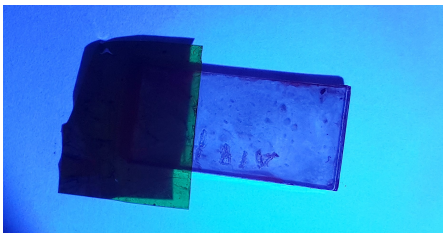 (b) 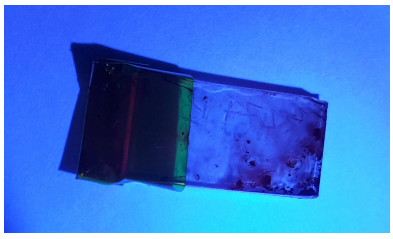

Fig. S16: Photos of C18 capped MAPI NCs deposited on a FTO coated glass under UV-light illumination; (a) Film with no annealing step (b) Film after thermal annealing at 100°C for 10 min. The photoluminescence properties of the films did not change

Bibliography

[1] E. Wang, Z. Ma, Z. Zhang, P. Henriksson, O. Inganäs, F. Zhang, and M. R. Andersson, "An isoindigo-based low band gap polymer for efficient polymer solar cells with high photo-voltage," *Chemical Communications*, vol. 47, no. 17, p. 4908, 2011.